STRENGTH ANALYSIS OF SANDWICH BEAMS WITH LINEAR ELASTIC INNER LAYER

Koichi Kimura

Maintenance Department, Kansai Depot, Japan Ground Self Defense Force
Gokasho, Uji-City, Kyoto 611-0011, Japan
jbt2222@infoseek.jp

Abstract. A waterproof or water-resistant sandwich structure which consists of housing chassis and a gasket requires that gasket contact pressure, which depends on bolt axial force, is greater than the design minimum pressure on the entire circumference. However, it is also necessary that gasket contact pressure is smaller than the maximum permissible gasket pressure. If the maximum stress in chassis can be calculated from bolt axial force, gasket specifications and chassis stiffness, it is helpful for a design of such waterproof structures. In this study, chassis have been regarded as Bernoulli-Euler beams, and two simple numerical methods have thus been derived. Numerical results using the proposed method are sufficiently converged even in case that the number of partitions is about 10.

1. Introduction

In order to achieve the waterproof property of precision equipment products and so on, sandwich structures which consist of housing chassis and a gasket between them are frequently applied. For waterproofing sandwich structures as shown in Figure 1, it is required that the gasket contact pressure is greater than the design minimum pressure (*y*-value) on the entire circumference. However, when the magnitude of bolt axial force, which governs gasket contact pressure, is too large, various problems may occur. Concretely, it is necessary that the bolt axial force is in range such that plastic deformation of chassis is not caused and that gasket contact pressure is smaller than the maximum pressure permissible to prevent gasket overdeformation. Hence, in order to set the bolt axial force to the optimum value, gasket characteristics and chassis strength shall be taken into account. By being able to compute the maximum stress in chassis from bolt axial force, gasket elastic modulus and chassis stiffness, we can also determine chassis stiffness from gasket specifications and vice versa.
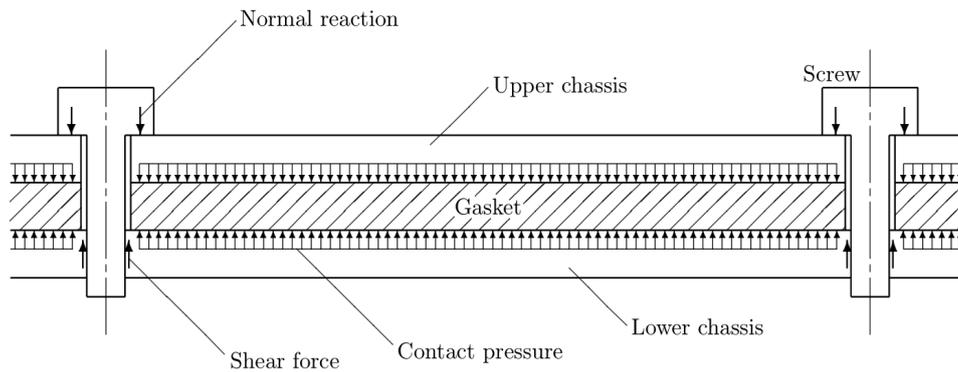
Fig. 1. Gasket and housing chassis

In this study, chassis have been regarded as Bernoulli-Euler beams with a uniform cross section, two methods of a classical approach in which the problem is analyzed by replacing the contact pressure with several point loads and an application of the boundary element method [1] have been derived, and numerical calculations and a comparative consideration have been carried out. As for sandwich beams, a considerable number of studies have been conducted, and various techniques have been proposed, since Hoff and Mautner [2] analyzed this problem using the energy method. Kenmochi and Uemura [3, 4] applied the multi-layer built-up theory to cases where the bending rigidity of core material could not be neglected. Eigenvalue problems of sandwich beams made of two elastic faces and a viscoelastic core were treated by Sato et al. [5] and Galucio et al. [6]. Cases where the Winkler model could be applied similarly to this paper, as the bending rigidity of core was very small, were also dealt with [7, 8]. In addition, in recent years, various studies on the mechanical behaviour of sandwich structures were reported [9–16]. In parallel with the development of digital computer technology, several studies have also been made on the bending analysis of elastic beams using the boundary element method [17–19]. The purpose of this study is to provide a practical guide for the design of sandwich structures which consist of housing chassis and a gasket, and the analytical model has been simplified in several ways. The bending rigidity of the equivalent beam can be mostly identified from the material and shape of a chassis. A gasket of which the width and thickness are uniform may be regarded as a 1-dimensional element, and the Winkler model can be applied since the rigidity is sufficiently small compared with those of chassis. In order to solve this problem, convenient methods in which a distributed load is replaced with many point loads, including the boundary element method, have been utilized. The uses of these methods are easier than getting the analytical solution of a contact pressure, and the influence of discretization of a distributed load on the numerical results of beam stresses and deflections was minimal.

2. Basic equations

The bending problem for beams as shown in Figure 2 is governed by the following differential equation [20–22]:

$$\frac{d^4 y_j(x)}{dx^4} = \frac{f(x)}{E_j I_j} \qquad (j = 1, 2) \tag{1}$$

where y_1 is the downward deflection of the lower beam (beam-1), y_2 is the upward deflection of the upper beam (beam-2), each E_j is Young's modulus of beam-1 or -2, each I_j is the moment of inertia of the cross-sectional area of beam-1 or -2, and $f(x)$ is the gasket reaction per unit length. Assuming that the reaction of the gasket at an arbitrary point is in proportion to compression deformation amount of the gasket at the same position, $f(x)$ is expressed by

$$f(x) = k\left[y_0 - y_1(x) - y_2(x)\right] \tag{2}$$

where k is the elastic modulus dependent on material and shape of the gasket, and y_0 is the compression deformation amount of the gasket at $x = l$. From the equilibrium of forces of the system in vertical direction, the relation between $f(x)$ and axial force P becomes the following equation:

$$P/2 = \int_0^l f(x)\,dx \tag{3}$$

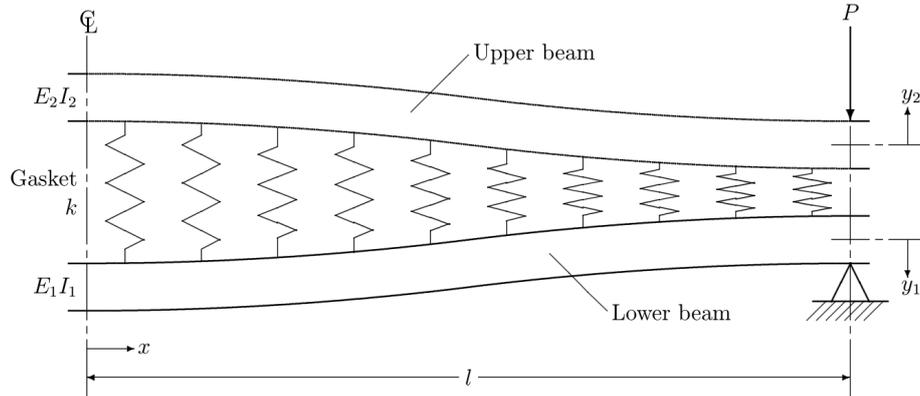where l is the half distance between supporting points.

Fig. 2. A schematic of double-beam system with elastic inner layer

3. Classical approach

Expressing the contact pressure at $x = e$ as $f(e)$, the deflections of beams-1 and -2 are given by the expression

$$y_j(x) = \int_0^l H_j(e,x) f(e) \, de \qquad (j = 1, 2) \tag{4}$$

where $H_j(e,x)$ are the deflections of the clamped-clamped beams subjected to unit concentrated loads at two symmetric points $x = \pm e$. From the beam bending theory [13–15], $H_j(e,x)$ ($j = 1, 2$) are given by

$$H_{jI}(e,x) = \frac{1}{12E_j I_j l}(l-e)^2(-3x^2 + 2el + l^2) \qquad (-e \leq x \leq e) \tag{5}$$

$$H_{jO}(e,x) = \frac{1}{12E_j I_j l}[2lx^3 - 3(l^2 + e^2)x^2 + 6e^2 lx + (l^2 - 3e^2)l^2]$$
$$(x \leq -e, e \leq x) \tag{6}$$

where $H_{jI}(e,x)$ and $H_{jO}(e,x)$ are the inner and outer deflections of beam-j subjected to unit point loads at two points $x = \pm e$, respectively. Substituting Eq. (4) into Eq. (2), we obtain

$$f(x) = k \left\{ y_0 - \int_0^l [H_1(e,x) + H_2(e,x)] f(e) \, de \right\} \tag{7}$$

In this section, in order to integrate Eqs. (3) and (7) numerically, equations

$$P/2 = \sum_{i=1}^{N} f(e_i) \Delta e \tag{8}$$

$$f(x) = k \left\{ y_0 - \sum_{i=1}^{N} [H_1(e_i,x) + H_2(e_i,x)] f(e_i) \Delta e \right\} \tag{9}$$

where $\Delta e = l/N$, $e_i = (2i-1)\Delta e/2$, and N is the number of partitions are adopted. Setting the calculation positions of contact pressure at e_i ($i = 1, 2, \ldots, N$), and satisfying Eq. (8) and Eq. (9) at $x = e_1, e_2, \ldots, e_N$, the simultaneous algebraic equations with $N+1$ unknowns are obtained. By solving these simultaneous equations, $f(e_i)$ and y_0 can be found. The approximate solutions of the beam deflections can be calculated from the following equation:

$$y_j(x) = \sum_{i=1}^{N} H_j(e_i,x) f(e_i) \Delta e \qquad (j = 1, 2) \tag{10}$$

In the present method, since the contact pressure, which is actually a distributed load, is replaced with a lot of point loads, derivatives of orders greater than or equal to 3 of Eq. (10) are not continuous functions. Hence, in order to get shearing forces, which require third-order derivatives of deflection functions, the third derivatives are found by numerically differentiating the beam deflections obtained by the present method. The stresses σ_j on the bottom surface of beam-1 and the top surface of beam-2, expressed by the following equation, can be acquired as continuous values by differentiating Eq. (10) twice

$$\sigma_j = \frac{M_j t_j}{2I_j} = -\frac{E_j t_j}{2}\left(\frac{d^2 y_j}{dx^2}\right) = -\frac{E_j I_j}{Z_j}\left(\frac{d^2 y_j}{dx^2}\right) \qquad (j = 1, 2) \tag{11}$$

where each t_j is the thickness of beam-1 or -2, and each Z_j is the section modulus of beam-1 or -2.

4. Application of boundary element method

In order to solve the differential equation (1), we start the boundary element method formulation from the following weighted residual form of

$$\int_0^l \left(\frac{d^4 y_j}{dx^4} - \frac{f(x)}{E_j I_j}\right) y_j^* \, dx \qquad (j = 1, 2) \tag{12}$$

Let us transform it through integration by parts. Here, l is the length of the span, and y_j^* are the weight functions selected according to the characteristic of becoming the delta function by differentiating four times. It is defined as a function of the distance between a source point ξ and a field point x [1]:

$$y_j^*(\xi, x) = \frac{1}{12 E_j I_j}(2L^3 + r^3 - 3Lr^2) \tag{13}$$

where $r = |x - \xi|$. After integrating Eq. (12) by parts four times, the equation of deflections at a point ξ within the domain is obtained utilizing the property of the delta function

$$y_j(\xi) = \left[y_j^*(\xi, x)V_j(x) - T_j^*(\xi, x)M_j(x) + M_j^*(\xi, x)T_j(x)\right.$$
$$\left. - V_j^*(\xi, x)y_j(x)\right]_{x=0}^{x=l} + \int_0^l f(x)y_j^*(\xi, x)\, dx \qquad (j = 1, 2) \tag{14}$$

Here, T_j are angles of deflections of the beams, M_j are the bending moments of the beams, and V_j are the shearing forces of the beams, which are related to the derivatives of deflections as follows:

$$T_j = \frac{dy_j}{dx}, \qquad M_j = -E_j I_j \frac{d^2 y_j}{dx^2}, \qquad V_j = -E_j I_j \frac{d^3 y_j}{dx^3} \tag{15}$$

The quantities marked with an asterisk * also have a similar relationship with the above with regard to y_j^*. It can be seen that Eq. (14) is described using 8×2 values of y_j, T_j, M_j and V_j at both ends ($x = 0$, l). Eight of these values are designated by boundary conditions at both ends, while the rest are unknown. Accordingly, eight independent equations are required to determine these unknown values. Four of them are given from Eq. (14) by letting $\xi \to 0$ and $\xi \to l$. The remaining four are usually obtained using the equation of angles of deflections. Differentiating Eq. (14) with respect to ξ, the equation of angles is obtained as

$$T_j(\xi) \equiv \frac{dy_j(\xi)}{d\xi} = \left[\tilde{y}_j^*(\xi,x) V_j(x) - \tilde{T}_j^*(\xi,x) M_j(x) + \tilde{M}_j^*(\xi,x) T_j(x) \right.$$
$$\left. - \tilde{V}_j^*(\xi,x) y_j(x) \right]_{x=0}^{x=l} + \int_0^l f(x) \tilde{y}_j^*(\xi,x) \, dx \qquad (j = 1, 2) \qquad (16)$$

The same operations letting $\xi \to 0$ and $\xi \to l$ in the above yield four more equations. We can then solve them as a system of simultaneous equations for the eight unknown values. After that, the deflections and the angles at an interior point ξ can be calculated from Eqs. (14) and (16), respectively. Equations of bending moments M_j and shearing forces V_j at point ξ are obtained, according to demand, by differentiating Eq. (16).

The fundamental solutions for the above beam flexure are given by Eq. (13) and the following equations:

$$T_j^*(\xi,x) = \frac{dy_j^*(\xi,x)}{dx} = \frac{1}{4E_jI_j} r(r - 2L) \operatorname{sgn}(x - \xi) \qquad (17)$$

$$M_j^*(\xi,x) = -E_jI_j \frac{d^2y_j^*(\xi,x)}{dx^2} = -\frac{1}{2}(r - L) \qquad (18)$$

$$V_j^*(\xi,x) = -E_jI_j \frac{d^3y_j^*(\xi,x)}{dx^3} = -\frac{1}{2} \operatorname{sgn}(x - \xi) \qquad (19)$$

and

$$\tilde{y}_j^*(\xi,x) = \frac{\partial y_j^*(\xi,x)}{\partial \xi} = -\frac{1}{4E_jI_j} r(r - 2L) \operatorname{sgn}(x - \xi) \qquad (20)$$

$$\tilde{T}_j^*(\xi,x) = \frac{\partial T_j^*(\xi,x)}{\partial \xi} = -\frac{1}{2E_jI_j}(r - L) \qquad (21)$$

$$\tilde{M}_j^*(\xi,x) = \frac{\partial M_j^*(\xi,x)}{\partial \xi} = \frac{1}{2}\,\mathrm{sgn}(x-\xi) \tag{22}$$

$$\tilde{V}_j^*(\xi,x) = \frac{\partial V_j^*(\xi,x)}{\partial \xi} = 0 \tag{23}$$

where $\mathrm{sgn}(x-\xi) = 1$ when $x > \xi$, $\mathrm{sgn}(x-\xi) = -1$ when $x < \xi$, and $\mathrm{sgn}(x-\xi)$ is undefined when $x = \xi$. Here, L may be set to the span length l and may also be set to zero.

In this section, in order to integrate Eqs. (2) and (3) numerically, equation

$$f(\xi) = k\left[y_0 - y_1(\xi) - y_2(\xi)\right] \tag{24}$$

where

$$y_j(\xi) = \left[y_j^*(\xi,x)V_j(x) - T_j^*(\xi,x)M_j(x) + M_j^*(\xi,x)T_j(x)\right.$$
$$\left. - V_j^*(\xi,x)y_j(x)\right]_{x=0}^{x=l} + \sum_{i=1}^{N} f(e_i)y_j^*(\xi,e_i)\Delta e \qquad (j=1,2) \tag{25}$$

and Eq. (8) are applied. Setting the contact pressure calculation positions at e_i ($i = 1$, $2, \ldots, N$), and satisfying Eq. (8) and Eq. (24) at $x = e_1, e_2, \ldots, e_N$, the simultaneous algebraic equations with $N+1$ unknowns are obtained. Next, in order to determine $y_j(0)$, $M_j(0)$, $M_j(l)$ and $V_j(l)$ ($j = 1, 2$) in Eq. (25), we consider the case of $\xi \to 0$ and $\xi \to l$ in Eq. (25) and its derivative with respect to ξ. Assuming that ε is a small positive constant, the following eight equations are obtained.

$$\begin{Bmatrix} y_j(0) \\ 0 \end{Bmatrix} = \begin{bmatrix} y_j^*(\varepsilon,l) & -T_j^*(\varepsilon,l) & M_j^*(\varepsilon,l) & -V_j^*(\varepsilon,l) \\ y_j^*(l-\varepsilon,l) & -T_j^*(l-\varepsilon,l) & M_j^*(l-\varepsilon,l) & -V_j^*(l-\varepsilon,l) \end{bmatrix}$$

$$\times \begin{Bmatrix} V_j(l) \\ M_j(l) \\ 0 \\ 0 \end{Bmatrix} - \begin{bmatrix} y_j^*(\varepsilon,0) & -T_j^*(\varepsilon,0) & M_j^*(\varepsilon,0) & -V_j^*(\varepsilon,0) \\ y_j^*(l-\varepsilon,0) & -T_j^*(l-\varepsilon,0) & M_j^*(l-\varepsilon,0) & -V_j^*(l-\varepsilon,0) \end{bmatrix}$$

$$\times \begin{Bmatrix} 0 \\ M_j(0) \\ 0 \\ y_j(0) \end{Bmatrix} + \sum_{i=1}^{N} \begin{Bmatrix} f(e_i)y_j^*(\varepsilon,e_i) \\ f(e_i)y_j^*(l-\varepsilon,e_i) \end{Bmatrix}\Delta e \qquad (j=1,2) \tag{26}$$

$$
\left\{ \begin{array}{c} 0 \\ 0 \end{array} \right\} = \left[\begin{array}{cccc} \tilde{y}_j^*(\varepsilon,l) & -\tilde{T}_j^*(\varepsilon,l) & \tilde{M}_j^*(\varepsilon,l) & -\tilde{V}_j^*(\varepsilon,l) \\ \tilde{y}_j^*(l-\varepsilon,l) & -\tilde{T}_j^*(l-\varepsilon,l) & \tilde{M}_j^*(l-\varepsilon,l) & -\tilde{V}_j^*(l-\varepsilon,l) \end{array} \right]
$$

$$
\times \left\{ \begin{array}{c} V_j(l) \\ M_j(l) \\ 0 \\ 0 \end{array} \right\} - \left[\begin{array}{cccc} \tilde{y}_j^*(\varepsilon,0) & -\tilde{T}_j^*(\varepsilon,0) & \tilde{M}_j^*(\varepsilon,0) & -\tilde{V}_j^*(\varepsilon,0) \\ \tilde{y}_j^*(l-\varepsilon,0) & -\tilde{T}_j^*(l-\varepsilon,0) & \tilde{M}_j^*(l-\varepsilon,0) & -\tilde{V}_j^*(l-\varepsilon,0) \end{array} \right]
$$

$$
\times \left\{ \begin{array}{c} 0 \\ M_j(0) \\ 0 \\ y_j(0) \end{array} \right\} + \sum_{i=1}^{N} \left\{ \begin{array}{c} f(e_i)\tilde{y}_j^*(\varepsilon,e_i) \\ f(e_i)\tilde{y}_j^*(l-\varepsilon,e_i) \end{array} \right\} \Delta e \qquad (j=1,2) \qquad (27)
$$

By solving those simultaneous equations with $N+9$ unknowns, $f(e_i)$, $y0$, $y_j(0)$, $M_j(0)$, $M_j(l)$ and $V_j(l)$ can be found. The beam deflections are analytically obtained as continuous functions from Eq. (25). Here, if ε is smaller than $l/10^n$ (n is the number of significant decimal digits on computer and about 15 in double), the loss of trailing digits [23, 24] may occur. Signs of the fundamental solutions (19) and (22) may thus become the opposites of right. Hence, the value of ε must be set, considering the number of significant digits on the computer.

The stresses σ_j on the bottom surface of beam-1 and the top surface of beam-2 expressed by Eq. (11) can be obtained as continuous functions by differentiating Eq. (25) twice. The second derivative of Eq. (25) is

$$
\frac{d^2 y_j(\xi)}{d\xi^2} = \frac{dT_j(\xi)}{d\xi} = \left[\frac{\partial \tilde{y}_j^*(\xi,x)}{\partial \xi} V_j(x) - \frac{\partial \tilde{T}_j^*(\xi,x)}{\partial \xi} M_j(x) + \frac{\partial \tilde{M}_j^*(\xi,x)}{\partial \xi} \right.
$$

$$
\left. \times T_j(x) - \frac{\partial \tilde{V}_j^*(\xi,x)}{\partial \xi} y_j(x) \right]_{x=0}^{x=l} + \sum_{i=1}^{N} f(e_i) \frac{\partial \tilde{y}_j^*(\xi,e_i)}{\partial \xi} \Delta e \qquad (j=1,2) \qquad (28)
$$

in which

$$
\frac{\partial^2 y_j^*(\xi,x)}{\partial \xi^2} = \frac{\partial \tilde{y}_j^*(\xi,x)}{\partial \xi} = \frac{1}{2E_j I_j}(r-L) \tag{29}
$$

$$
\frac{\partial^2 T_j^*(\xi,x)}{\partial \xi^2} = \frac{\partial \tilde{T}_j^*(\xi,x)}{\partial \xi} = \frac{1}{2E_j I_j} \mathrm{sgn}(x-\xi) \tag{30}
$$

$$
\frac{\partial^2 M_j^*(\xi,x)}{\partial \xi^2} = \frac{\partial \tilde{M}_j^*(\xi,x)}{\partial \xi} = 0 \tag{31}
$$

$$
\frac{\partial^2 V_j^*(\xi,x)}{\partial \xi^2} = \frac{\partial \tilde{V}_j^*(\xi,x)}{\partial \xi} = 0 \tag{32}
$$

5. Numerical results

Numerical calculations using the two solution methods shown in Sections 3 and 4 have been carried out, and it was proved that their numerical solutions were completely equal values by adopting the same methods for the discretization of contact pressure distribution and for numerical integration. In order to determine the number of partitions N, the convergence of the solution was investigated. As examples, the compression deformation amount $y_0 E_1 I_1/(Pl^3)$ of the gasket at $x = l$, the maximum deflection $y_j(0) E_1 I_1/(Pl^3)$ and the maximum absolute stress $-\sigma_j(l) t_1^3/(Pl)$ of the beam in the case of $kl^4/(E_1 I_1) = 1$, $E_2 I_2/(E_1 I_1) = 1$, $Z_1/t_1^3 = 1/6$ and $Z_2/Z_1 = 1$ were calculated, changing the number of partitions from $N = 2$ into 3, 4, 5, 10, ..., 100. From Table 1, it can be seen that the numerical solutions of displacements are fairly right values even in the case of $N = 2$, and the calculation result of stress is sufficiently converged in the case that the number of partitions N is about 10. Hence, numerical examples for the present problem were calculated in the number of partitions $N = 10$.

In order to achieve the waterproof property of a product, the condition that the contact pressures between the chassis and the gasket are greater than the design minimum pressure (y-value) on the entire circumference must be satisfied. Accordingly, first, an example of contact pressure distributions and the relation between the gasket-to-beam stiffness ratio and the minimum contact pressure is presented in graphical form. Figure 3 is a numerical example of distributions of the dimensionless contact pressure fl/P, and the relation between the gasket-to-beam stiffness ratio $kl^4/(E_1 I_1)$ and the minimum contact pressure $f(0) l/P$ is indicated in Figure 4. Since the higher the gasket elastic modulus is, the smaller the minimum contact pressure is, a greater axial force or necessary and sufficient elasticity of the gasket used is required. Figure 4 shows that as $E_2 I_2/(E_1 I_1)$ becomes larger, the curve of the present solutions approaches that of the exact solutions when $E_2 I_2 = \infty$, which is equivalent to a continuous beam on an elastic foundation [25], and thus it can be seen that the present calculation results are valid.

Table 1. Convergence of the solution [$kl^4/(E_1 I_1) = 1$, $E_2 I_2/(E_1 I_1) = 1$, $Z_1/t_1^3 = 1/6$, $Z_2/Z_1 = 1$]

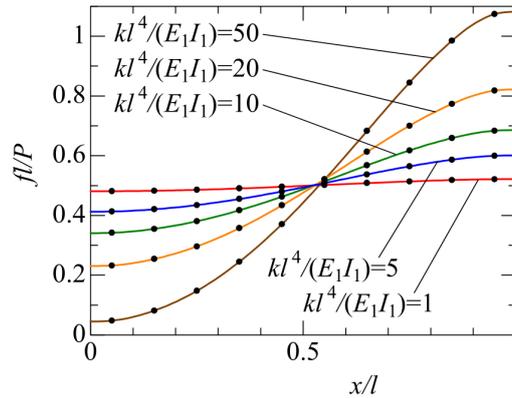| Number of partitions N	Numerical solutions		
	$y_0 E_1 I_1/(Pl^3)$	$y_j(0) E_1 I_1/(Pl^3)$	$-\sigma_j(l) t_1^3/(Pl)$
2	0.522059	0.020431	1.020727
3	0.521856	0.020422	1.002163
4	0.521823	0.020421	0.995743
5	0.521814	0.020420	0.992786
10	0.521808	0.020420	0.988858
20	0.521807	0.020420	0.987879
50	0.521807	0.020420	0.987605
100	0.521807	0.020420	0.987566

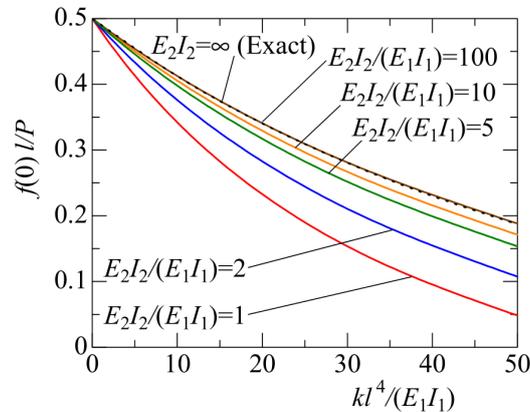Fig. 3. Contact pressure distributions $[E_2I_2/(E_1I_1) = 1]$

Fig. 4. Relationship between the gasket-to-beam stiffness ratio $kl^4/(E_1I_1)$ and the minimum contact pressure $f(0)l/P$

In Figures 5 and 6, the distributions of the deflections y_j and the surface stresses σ_j of the beams are indicated, respectively. As these are solutions to a problem involving Eq. (2), the deflection distributions are dependent upon the contact pressure distributions. As k becomes smaller, the curves of the present solutions approach those of the exact solutions when $k = 0$, which is equivalent to a uniformly loaded clamped beam [20], and thus it can be seen that the present calculation results are valid. In the present methods, since the contact pressure, which is actually a distributed load, is replaced with point loads, the stress distributions are obtained as continuous functions which have kinks at calculation points $x = e_1, e_2, ..., e_N$. As can be seen from Figure 6, the maximum absolute stresses appeared at a position $x = l$ subjected to bolt axial force. Hence, in chassis design, by increasing the stiffness as it approaches a position of bolt hole, chassis strength can be raised efficiently.
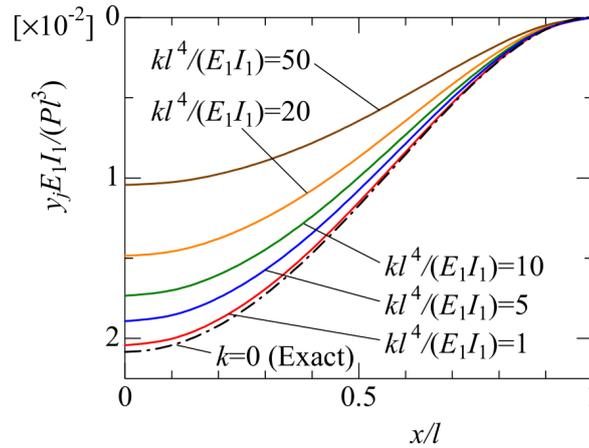
Fig. 5. Deflection distributions $[E_2I_2/(E_1I_1) = 1]$
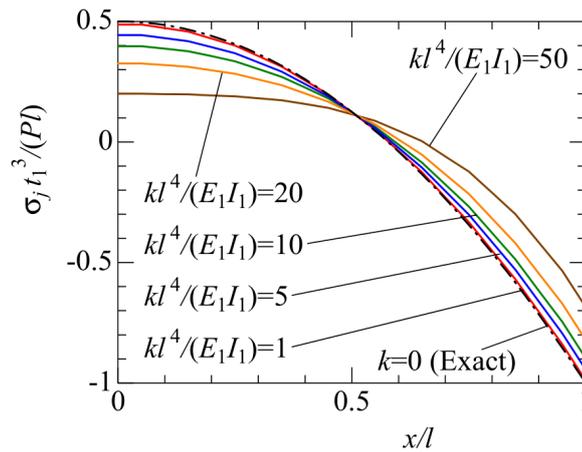
Fig. 6. Surface stress distributions $[E_2I_2/(E_1I_1) = 1, Z_1/t_1^3 = 1/6, Z_2/Z_1 = 1]$

In Figure 7, the relation between the maximum absolute stress $-\sigma_j(l)\,t_1^3/(Pl)$ and the beam flexural rigidity ratio $E_2I_2/(E_1I_1)$ in the case that lower and upper beams have the same Young's modulus and rectangular cross sections of the same width is indicated. As $E_2I_2/(E_1I_1)$ becomes larger, the present solutions are asymptotically close to the exact solutions when $E_2I_2 = \infty$, and thus it can be seen that the effect of stiffness ratio between two beams and a gasket on the calculation results has been correctly evaluated. The maximum absolute stress on the greater side of the beam flexural rigidity is smaller than that on the other side. Thus, focusing on the beam on the smaller side of the flexural rigidity, design computation should be carried out.
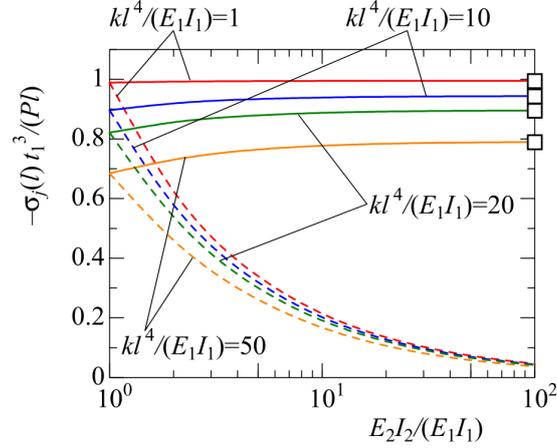
Fig. 7. Relationship between the maximum absolute stress $-\sigma_j(l)\,t_1{}^3/(Pl)$ and the beam flexural rigidity ratio $E_2I_2/(E_1I_1)$ $[Z_1/t_1{}^3 = 1/6, Z_2/Z_1 = [E_2I_2/(E_1I_1)]^{2/3}]$: solid curves, beam-1; dashed curves, beam-2; squares, beam-1 on elastic foundation ($E_2I_2 = \infty$)

6. Conclusions

Numerical methods for deflections and stresses of sandwich beams with a linear elastic inner layer have been suggested. Substituting the model for a sandwich structure which consists of housing chassis and a gasket, and using those numerical methods, the maximum stress in chassis can be calculated from bolt axial force, gasket elastic modulus and chassis stiffness.

The following conclusions can be drawn from this analysis:

1. The numerical result of stress presented in Table 1 is sufficiently converged in case that the number of partitions is about 10. By using the present methods, the deflections and stresses of a sandwich beam with linear elastic inner layer can be easily obtained in a comparatively small number of discretization nodes. From comparisons with the exact solutions when $k = 0$ and when $E_2I_2 = \infty$, it can be regarded that the present calculation results are correct.

2. Though the stress distributions are obtained as continuous functions, they have kinks at calculation points. By increasing the number of partitions, the influence of discretization becomes weaker, and sufficiently smooth curves of the stress distributions can be obtained even in case that the number of partitions is about 10.

3. In chassis design, by increasing the stiffness as it approaches a position of bolt hole, chassis strength can be raised efficiently. Even though the stiffness of a face beam is non-uniform, the present numerical method becomes available for strength analysis by using suitable beam deflection equations (e.g., Eqs. (2) and (3) in Ref. 26 for a bilateral symmetrically tapered beam) instead of Eqs. (5) and (6).

Acknowledgements

The author is grateful to Professor Emeritus Masaaki Okamoto of Osaka Electro-Communication University for his kindness and instruction.

References

[1] Butterfield, R. (1979). New concepts illustrated by old problems. *Developments in Boundary Element Methods*, Vol. 1. London: Applied Science Publishers Ltd., 1-20.

[2] Hoff, N.J., & Mautner, S.E. (1948). Bending and buckling of sandwich beams. *Journal of the Aeronautical Sciences*, *15*(12), 707-720.

[3] Kenmochi, K. (1978). Deflection of sandwich beams. *Journal of the Japan Society for Composite Materials*, *4*(1), 39-44 (in Japanese).

[4] Kenmochi, K., & Uemura, M. (1978). Discussion of four-point bending stress in sandwich composite beam by multi-layer built-up theory. *Journal of the Society of Materials Science, Japan*, *27*(299), 728-734 (in Japanese).

[5] Sato, K., Shikanai, G., & Tainaka, T. (1986). Damping of flexural vibration of viscoelastic sandwich beam subjected to axial force. *Bulletin of JSME*, *29*(253), 2204-2210.

[6] Galucio, A.C., Deü, J.-F., & Ohayon, R. (2004). Finite element formulation of viscoelastic sandwich beams using fractional derivative operators. *Computational Mechanics*, *33*(4), 282-291.

[7] Hassinen, P., & Martikainen, L. (1994). Analysis and design of continuous sandwich beams. *Proc. of 12th International Specialty Conference on Cold-Formed Steel Structures*, 523-538.

[8] Mirzabeigy, A., & Madoliat, R. (2019). A note on free vibration of a double-beam system with nonlinear elastic inner layer. *Journal of Applied and Computational Mechanics*, *5*(1), 174-180.

[9] Zhang, J., Qin, Q., Xiang, C., Wang, Z., & Wang, T.J. (2016). A theoretical study of low-velocity impact of geometrically asymmetric sandwich beams. *International Journal of Impact Engineering*, *96*, 35-49.

[10] Zhang, J., Qin, Q., Xiang, C., & Wang, T.J. (2016). Dynamic response of slender multilayer sandwich beams with metal foam cores subjected to low-velocity impact. *Composite Structures*, *153*, 614-623.

[11] Zhang, J., Ye, Y., Qin, Q., & Wang, T. (2018). Low-velocity impact of sandwich beams with fibre-metal laminate face-sheets. *Composites Science and Technology*, *168*, 152-159.

[12] Zhang, J., Qin, Q., & Wang, T.J. (2013). Compressive strengths and dynamic response of corrugated metal sandwich plates with unfilled and foam-filled sinusoidal plate cores. *Acta Mechanica*, *224*, 759-775.

[13] Zhang, J., Liu, K., Ye, Y., & Qin, Q. (2019). Low-velocity impact of rectangular multilayer sandwich plates. *Thin-Walled Structures*, *141*, 308-318.

[14] Zhang, J., Qin, Q., Zhang, J., Yuan, H., Du, J., & Li, H. (2021). Low-velocity impact on square sandwich plates with fibre-metal laminate face-sheets: Analytical and numerical research. *Composite Structures*, *259*, 113461.

[15] Zhang, J., Zhu, Y., Li, K., Yuan, H., Du, J., & Qin, Q. (2022). Dynamic response of sandwich plates with GLARE face-sheets and honeycomb core under metal foam projectile impact: Experimental and numerical investigations. *International Journal of Impact Engineering*, *164*, 104201.

[16] Zhang, J., Ye, Y., Zhu, Y., Yuan, H., Qin, Q., & Wang, T.J. (2020). On axial splitting and curling behaviour of circular sandwich metal tubes with metal foam core. *International Journal of Solids and Structures*, *202*, 111-125.

[17] Mendonça, A.V., & Nascimento Jr, P.C. (2013). Boundary element formulation for the classical laminated beam theory. *22nd International Congress of Mechanical Engineering*, 2256-2262.

[18] Carrer, J.A.M., Mansur, W.J., Scuciato, R.F., & Fleischfresser, S.A. (2014). Analysis of Euler--Bernoulli and Timoshenko beams by the boundary element method. *Proc. 10th World Congr. Comput. Mech.*, 2333-2349.

[19] Tsiatas, G.C., Siokas, A.G., & Sapountzakis, E.J. (2018). A layered boundary element nonlinear analysis of beams. *Frontiers in Built Environment*, *4*, 52.

[20] Timoshenko, S. (1955). *Strength of Materials, Part 1: Elementary Theory and Problems*, 3rd ed. New York: Van Nostrand, 137-175.

[21] Prescott, J. (1924). *Applied Elasticity*. London: Longmans, Green and Co., 47-78.

[22] Dym, C.L., & Shames, I.H. (1973). *Solid Mechanics: A Variational Approach*. New York: McGraw-Hill, 174-241.

[23] Natori, M. (1990). *Numerical Analysis and its Applications*. Tokyo: Corona Publishing Co., Ltd., 6-11 (in Japanese).

[24] Okumura, H. (2018). *Standard Dictionary of Algorithms in C*. Rev. ed. Tokyo: Gijutsu-Hyohron Co., Ltd., 128 (in Japanese).

[25] Timoshenko, S. (1956). *Strength of Materials, Part 2: Advanced Theory and Problems*, 3rd ed. New York: Van Nostrand, 1-25.

[26] Kimura, K., Okamoto, M., & Uemura, K. (2007). Bending of uniformly loaded circular plates supported by a tapered cross stiffener. *Journal of Strain Analysis for Engineering Design*, *42*(8), 581-588.